Solar Energy Materials and Solar Cells 171 (2017) 180–186

Contents lists available at ScienceDirect

Solar Energy Materials and Solar Cells

journal homepage: www.elsevier.com/locate/solmat

Optimized multicrystalline silicon for solar cells enabling conversion efficiencies of 22%

Florian Schindler[a,*], Bernhard Michl[a,1], Patricia Krenckel[a,1], Stephan Riepe[a,1], Jan Benick[a,1], Ralph Müller[a,1], Armin Richter[a,1], Stefan W. Glunz[a,b,1], Martin C. Schubert[a,1]

[a] Fraunhofer Institute for Solar Energy Systems (ISE), Heidenhofstr. 2, 79110 Freiburg, Germany
[b] University Freiburg, Laboratory for Photovoltaic Energy Conversion, Freiburg, Germany

ARTICLE INFO

Keywords:
Multicrystalline silicon
N-type
Efficiency limiting bulk recombination analysis
TOPCon
Resistivity

ABSTRACT

Multicrystalline (mc) *n*-type silicon has proven to be a suitable substrate for the fabrication of highly efficient mc-Si solar cells. In this paper, we elaborate the impact of base material parameters on the efficiency potential of *n*-type mc-Si solar cells featuring a boron-diffused front side emitter and a full-area passivating rear contact (TOPCon). The electrical material quality can be significantly improved by replacing the standard crystallization process with a seed-assisted growth for crystallization of high-performance (HP) mc silicon. Using high-purity quartz crucibles or larger crucibles in combination with an optimization of the grain boundary area fraction with an adapted seed structure leads to further improvements of the material quality in terms of charge carrier lifetimes. However, not only the charge carrier lifetime, but also the base resistivity is of crucial importance for the efficiency potential depending on the cell concept. Based on experimental data and simulations, we assess the optimal range for the base resistivity and the wafer thickness for *n*-type mc-Si TOPCon solar cells. With the optimal material parameters, an "efficiency limiting bulk recombination analysis" (ELBA) reveals an efficiency potential in the range of 22.5% for *n*-type mc-Si TOPCon solar cells. Finally, we fabricated TOPCon solar cells based on optimized *n*-type HP mc-Si substrate and demonstrate a certified efficiency of 21.9%, which is the highest efficiency reported for multicrystalline silicon solar cells so far.

1. Introduction

With progress in crystallization techniques, such as seed-assisted growth for the fabrication of so called "high-performance" (HP) multicrystalline (mc) silicon [1], the material quality of mc-Si wafers has increased significantly in the past years, mainly due to a reduced density of recombination-active dislocation clusters. Higher quality mc-Si substrates in combination with advancements in solar cell architectures resulted in a new certified world record mc-Si solar cell featuring an efficiency of 21.3% [2,3]. Like all industrially fabricated mc-Si solar cells, this record cell is based on *p*-type mc-Si substrate. However, the highest silicon solar cell efficiencies on monocrystalline silicon are achieved on *n*-type substrate, such as the current records of 26.6% [4] and 25.3% [5] for heterojunction and homojunction cells, respectively. Due to the smaller impact of many metal impurities, such as interstitial iron, on the electrical material quality [6] and the absence of the boron-oxygen-related degradation [7,8], *n*-type doping could also be a promising option for multicrystalline silicon solar cells, if an appropriate cell concept is provided. We have recently shown that the TOPCon cell concept [9] featuring a boron-diffused front side emitter and a full-area passivating rear contact is applicable to *n*-type mc-Si substrate and demonstrated an efficiency of 19.6% [10]. A main limitation of this solar cell was the poor optics of the isotextured front surface, which capped the cell limit without bulk recombination losses to approximately 21%. With the development of a plasma-etched "black-silicon" texture in combination with further technological advancements, a cell process with a concept-related efficiency limit above 23% (without defect recombination losses) has been developed, which is applicable for the fabrication of *n*-type mc-Si TOPCon solar cells [11]. With regard to this high cell limit, the reduction of material-related efficiency losses in the mc-Si substrate becomes of utmost importance, which is the focus of this work. Based on experimental results in combination with simulations, we quantify efficiency gains from improvements of the crystal structure and the optimal choice of

* Corresponding author.
E-mail addresses: florian.schindler@ise.fraunhofer.de (F. Schindler), bernhard.michl@ise.fraunhofer.de (B. Michl), patricia.krenckel@ise.fraunhofer.de (P. Krenckel), stephan.riepe@ise.fraunhofer.de (S. Riepe), jan.benick@ise.fraunhofer.de (J. Benick), ralph.mueller@ise.fraunhofer.de (R. Müller), armin.richter@ise.fraunhofer.de (A. Richter), stefan.glunz@ise.fraunhofer.de (S.W. Glunz), martin.schubert@ise.fraunhofer.de (M.C. Schubert).
[1] Co-authors.

http://dx.doi.org/10.1016/j.solmat.2017.06.005
Received 12 April 2017; Received in revised form 2 June 2017; Accepted 5 June 2017
Available online 04 July 2017

Table 1
n-type mc-Si wafers.

	Crystallization	Crucible	Coating	Resistivity (Ω cm)
A	standard	G2 standard	ISE	2.0
B	HP	G1 HPC	Vesuvius	1.0
C	HP	G2 standard	Vesuvius	10.8
D	HP optimized	G2 standard	Vesuvius	0.75

parameters for resistivity and wafer thickness. Thus, we present a concept how to optimally exploit a cell's efficiency potential by minimizing material-related efficiency losses.

2. Material and methods

The development of *n*-type mc-Si materials at Fraunhofer ISE and their evaluation for the use in high-efficiency solar cells comprised standard directional solidification processes with nucleation of initial grains directly at the crucible bottom ("standard process") as well as materials with nucleation at seed materials ("high-performance process"). The ingots to be evaluated had either the laboratory size G1 equivalent to 15 kg of Si feedstock (supplied by Wacker Polysilicon) or laboratory size G2 equivalent to 75 kg. From both types of ingot center bricks were cut and further processed into wafers. In this study, we included four different *n*-type mc-Si materials, one from a standard crystallization process and three from high-performance (HP) crystallization processes with variations in the seed structure, the crucible systems as well as the base resistivity (*cf.* Table 1). Wafers were taken from the upper third of each ingot: wafer "A" stems from a standard crystallization process in a G2 size crucible of standard purity coated at ISE, wafers "B-D" are HP mc-Si wafers originating from seed-assisted growth crystallization processes. Material "B" was crystallized in a G1 size crucible of high purity (Vesuvius "high purity crucible" HPC with Vesuvius coating), wafers "C" and "D" in G2 size crucibles (Vesuvius standard crucibles with Vesuvius coating). Wafers "C" and "D" differ strongly in their resistivity. Further, for material "D" the seed-assisted growth was adapted in order to obtain an optimized grain boundary area fraction, featuring a sufficiently high amount of grain boundaries for the suppression of dislocation clusters, but favouring the growth of large grains at the same time. This was done by using a plate cut from a high-performance mc-Si ingot as seed layer in the crucible bottom instead of granular silicon. This plate features an optimal distribution of grain sizes such that largest possible grains develop along the entire ingot height without the emergence of recombination active dislocation clusters. For the high-performance wafers investigated here, the median grain sizes increase from ~ 9 mm^2 ("B") to ~ 24 mm^2 ("C") and ~ 36 mm^2 ("D").

It should be noted that the crystallization processes in terms of crystallization times and cooling ramps are identical for materials "C" and "D", whereas the other two differ either due to a different crucible size (G1 for material "B") or due to a different crystallization technique ("standard" instead of high-performance for material "A"). Of course, this also comes along with variations in the impurity content of the different materials [12]. As a change in the crystallization technique always requires changes in the processing parameters, it inherently involves differences in the impurity content of the crystallized materials. Thus, the results presented in this paper comprise the impact of combined effects arising from changes in the crystallization techniques.

The wafers were processed to lifetime samples by applying the high-temperature steps of a TOPCon solar cell process sequence, i.e. a boron diffusion at 890 °C and an annealing step at 800 °C (both for 1 h) (*cf.* Fig. 1). This ensures that the material quality of the lifetime samples corresponds to the material quality of the final cell and allows for an analysis of the material related efficiency losses. To obtain an injection-independent surface passivation, the wafers were passivated with SiN_x-films. Injection-dependent photoluminescence (PL) imaging calibrated by modulated PL [13] allows for spatially resolved characterization of the bulk minority charge carrier lifetime τ_{bulk} (in the following referred to as "bulk lifetime") and, in combination with PC1D [14,15] cell simulations, for a prediction of the cell efficiency potential by an "Efficiency limiting bulk recombination analysis" (ELBA) [16]. The latter additionally enables a detailed loss analyses as presented in [17]. The parameters for the PC1D model were taken from recombination current prefactor (J_0) measurements of the TOPCon rear side ($J_{0,rear}$ = 7 fA/cm^2), the black-silicon boron-diffused front side (J_{0e} = 65 fA/cm^2), reflection measurements of the front side (weighted reflection = 1%) [11], and base resistivity measurements of the mc-Si material. Furthermore, a series resistance of 0.55 Ω cm^2 was assumed. This leads to a cell limit without bulk recombination losses of 23.1%.

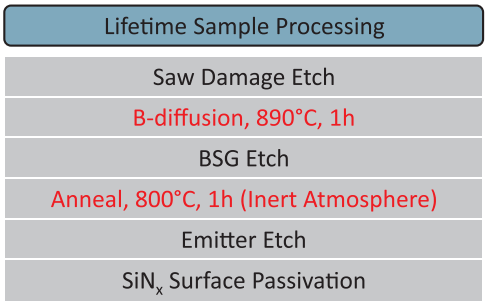

Fig. 1. Lifetime sample processing sequence. By choosing the high-temperature steps of a TOPCon solar cell process, we obtain lifetime samples with material quality corresponding to that of the TOPCon solar cells.

3. Results

3.1. Bulk lifetime

For a first evaluation of the material quality, Fig. 2(a) shows PL images of τ_{bulk} obtained at an irradiation of ~ 0.05 suns (~ corresponding to injection conditions at maximum power point, MPP) together with the average lifetime across the image. In the following, all average lifetime values are square root harmonic means, indicated by $\tau_{1/L}$. Wafer "A" from the standard crystallization process features some large grains of high bulk lifetime close to 1 ms. The clear drawback of this material are large areas featuring a high density of strongly recombination-active structural crystal defects such as grain boundaries and dislocation clusters, which limit the area averaged lifetime to 138 µs. The strongly recombination-active dislocation clusters can be avoided by seed-assisted growth, delivering high-performance multicrystalline silicon. In combination with use of a high purity crucible, this leads to smaller grains with higher bulk lifetimes. Thus, the average bulk lifetime is increased to 403 µs (wafer "B"). While the best grains of this material feature bulk lifetimes close to 2 ms, the average is still limited by a rather large amount of recombination-active grain boundaries. To reduce their impact, we followed two approaches: Material "C" features a higher resistivity (*cf.* Table 1), which leads to a reduced recombination at metallic precipitates [18], and for material "D" we adapted the seed-assisted growth such that an optimized grain boundary area fraction is obtained: on the one hand, it delivers a sufficiently high amount of grain boundaries for the suppression of dislocation clusters, on the other hand it favours the growth of still large grains.

Both materials "C" and "D" feature high inner grain bulk lifetimes exceeding 2.5 ms. Despite the virtually identical impurity content of these two materials and the even better crystal structure of wafer "D", the average bulk lifetime of wafer "C" (913 µs) is significantly higher than that of wafer "D" (634 µs), which is attributed to reduced recombination in the high resistivity wafer "C" due to a combination of the following effects:

(1) Lower intrinsic recombination (radiative and Auger).
(2) Lower Shockley-Read-Hall (SRH) recombination: A lower base

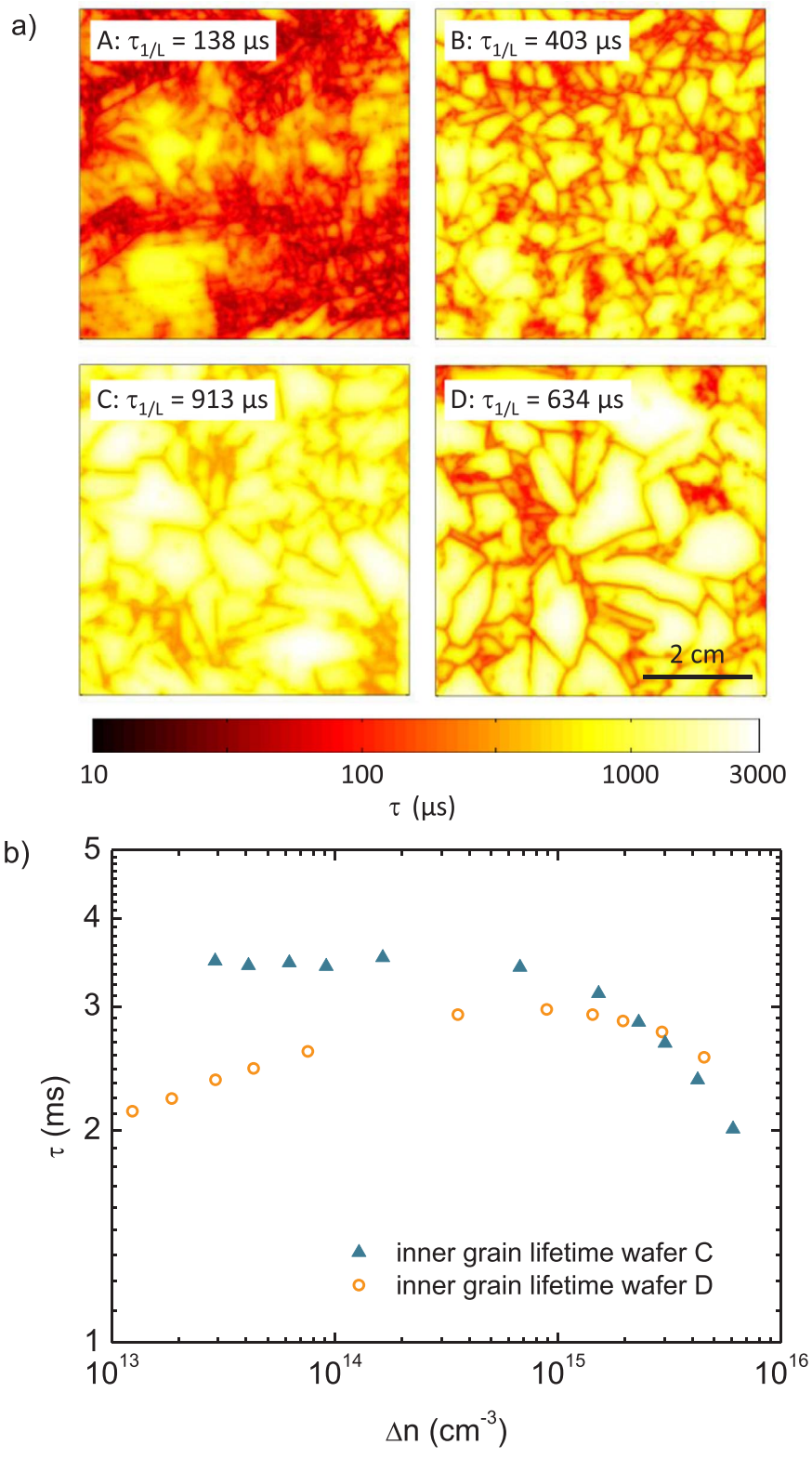

Fig. 2. a) Images of the bulk lifetime after the process sequence indicated in Fig. 1 at an irradiation of ~ 0.05 suns for *n*-type mc-Si wafers from different crystallizations (*cf.* Table 1: "A" standard mc-Si, "B" HP mc-Si, "C" high resistivity HP mc-Si, "D" HP mc-Si with optimized grain structure). An exceptionally high average bulk lifetime close to 1 ms and inner grain lifetimes in the range of 3 ms are achieved with material "C". b) Injection-dependent inner grain bulk lifetime of wafers "C" and "D". Whereas the high resistivity wafer "C" features virtually no injection-dependence towards low level injection, wafer "D" is affected by a stronger injection-dependence.

doping concentration leads to a shift of the entire $\tau(\Delta n)$-curve along the Δn-axis towards smaller Δn. Since for the majority of typical impurities an increased lifetime with increasing excess charge carrier density Δn is observed, this leads to higher lifetimes for identical Δn. However, as indicated by the injection-dependent lifetime measured in the grains of wafers "C" and "D" (*cf.* Fig. 2(b)), the lower inner-grain lifetime of wafer "D" cannot solely be explained by this shift, as wafer "C" features no significant injection-dependence towards low level injection.

(3) Lower recombination at metallic precipitates: A lower base doping concentration leads to a reduced charging of the metal precipitates with majority charge carriers and, thus, a reduced capture cross section for minority charge carriers [18].

While (1) is an effect which only depends on the charge carrier density, (2) leads to a reduced recombination in areas limited by

recombination at dissolved impurities, and (3) mainly leads to a lower recombination activity of grain boundaries decorated with metallic precipitates. Although the inner-grain lifetime of wafer "D" decreases with decreasing Δn, it is still on a high level above 2 ms and does not alone explain the significantly lower average lifetime compared with wafer "C". The dominant effect resulting in a higher average lifetime in wafer "C" is the lower recombination rate at and in the vicinity of grain boundaries, *i.e.* a combined effect of a lower recombination at metallic precipitates decorating the grain boundaries and a lower SRH recombination at dissolved impurities in their vicinities.

3.2. Efficiency loss analysis

From an isolated view at the bulk lifetime, one could assume that the high resistivity material "C" would perform best in a solar cell. However, even for a solar cell structure which shows only a relatively weak dependence on the base resistivity – such as the TOPCon concept – its impact becomes of importance for lower bulk quality material [19]. Whereas the bulk lifetime itself benefits from a higher resistivity as explained in the previous section, a lower resistivity is favourable for bulk-recombination limited TOPCon solar cells [19] – *i.e.* $\tau_{eff} \lesssim 3$ ms (*cf.* Fig. 2(g) in [19]), which is the case for all materials investigated here. This is due to the majority charge carrier concentration at MPP conditions being determined by the background doping rather than the excess charge carrier density under these conditions. Thus, a higher base doping concentration leads to a larger *np*-product and, consequently, a higher voltage at MPP conditions. Therefore, the trade-off between bulk lifetime and resistivity needs to be quantified for any specific cell concept of interest. In the following, this is done for the example of the TOPCon cell concept by an ELBA analysis.

Fig. 3(a) shows the predicted efficiency potential for the same four wafers presented in Fig. 2 in combination with the solar cell model described in section II featuring a cell limit of 23.1%. The corresponding material-related efficiency losses are plotted by the green and grey bars in Fig. 3(b), the orange bars will be referred to in the next section.

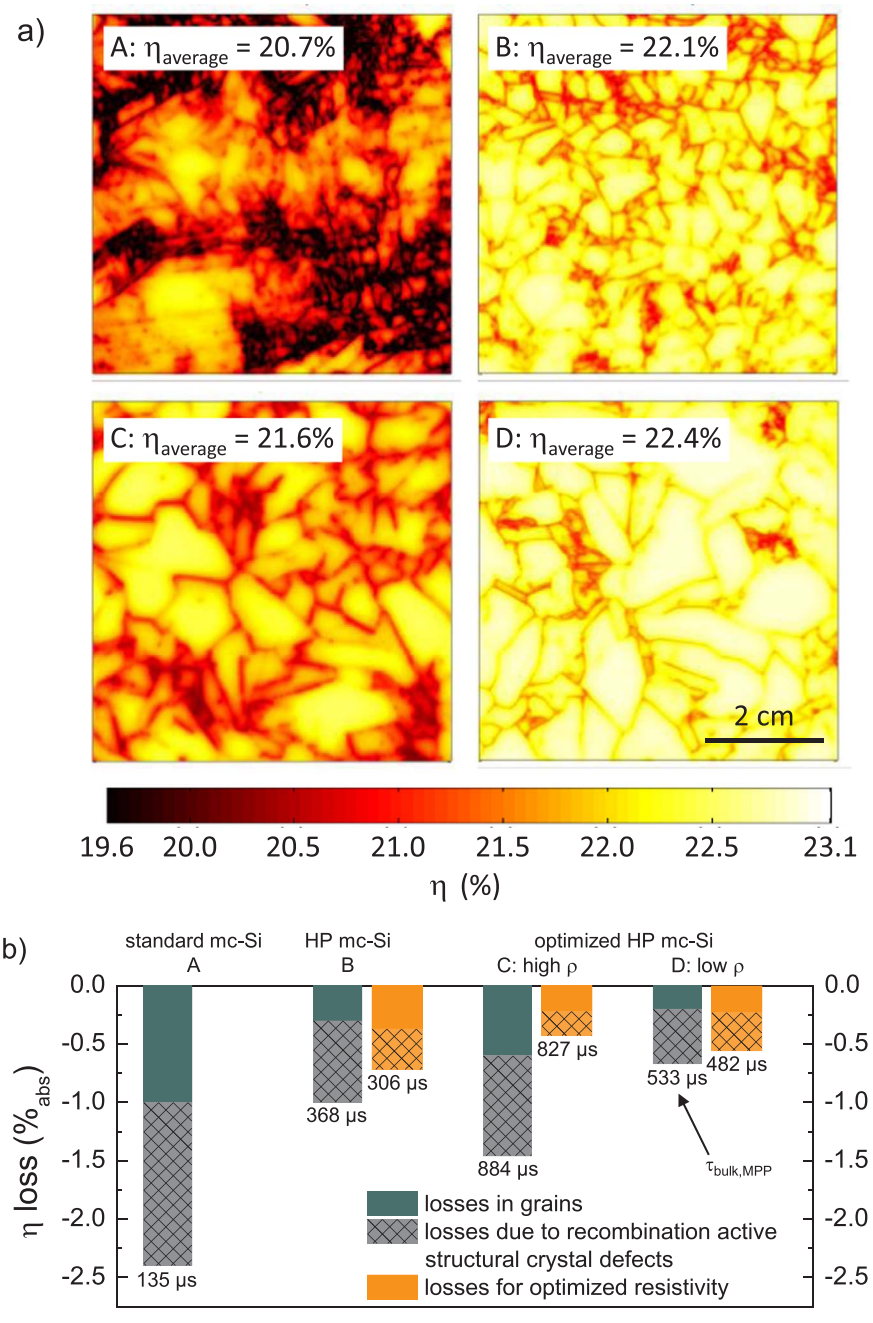

Fig. 3. a) ELBA prediction of the spatially resolved efficiency potential for the four wafers A–D. b) Corresponding solar cell efficiency losses. The green and grey bars refer to the actual losses, the orange bars to the simulated losses of the same material at optimized resistivity. With an improved crystal structure and an optimized base resistivity, material-related losses can be reduced to approximately $0.5\%_{abs}$. (For interpretation of the references to color in this figure legend, the reader is referred to the web version of this article).

Obviously, the largest efficiency losses of 2.4%$_{abs}$ are observed for the standard crystallization process ("A"). A TOPCon solar cell based on this substrate would be limited to an efficiency of ~ 20.7%. A strong reduction in efficiency losses can be achieved by making use of a high-purity crucible to reduce inner grain losses due to homogeneously distributed impurities together with the application of seed-assisted growth for the suppression of highly recombination-active dislocation clusters. Thus, the obtained high-performance mc-Si ("B") features efficiency losses of only ~ 1%$_{abs}$. However, as indicated by the grey meshed part of the second bar ("B") in Fig. 3(b), losses due to recombination-active structural crystal defects are still significant. In order to reduce these losses, we fabricated HP mc-Si material "D" with the adapted seed-assisted growth. This material features the lowest efficiency losses of ~ 0.7%$_{abs}$ (fourth bar in Fig. 3(b)), which results in a predicted efficiency potential of ~ 22.4% (*cf.* Fig. 3(a)).

As discussed in the previous section, material "C" features a significantly larger bulk lifetime than material "D" (884 µs compared to 533 µs at maximum power point (MPP); note that slight differences compared to the values from Fig. 2(a) are due to slightly different injection conditions at MPP compared to the injection conditions at ~ 0.05 suns in Fig. 2(a)). However, efficiency losses for wafer "C" are even larger than those for wafer "B" (*cf.* Fig. 3). This can be attributed to the rather high resistivity of this material (~ 11 Ω cm), which will be discussed in detail in the next section.

3.3. Optimization of base resistivity and wafer thickness

Besides high material quality in terms of high charge carrier lifetimes, the correct choice of base resistivity is crucial for the reduction of material-related efficiency losses. As demonstrated in the previous section, the high-resistivity material "C" (~ 11 Ω cm) features significantly larger efficiency losses (~ 1.5%$_{abs}$) despite its higher MPP bulk lifetime (884 µs) compared to material "D" (0.75 Ω cm, 533 µs, ~ 0.7%$_{abs}$). These results highlight the crucial impact of the correct choice of base resistivity for the fabrication of highly efficient *n*-type mc-Si TOPCon solar cells and suggest that choosing an optimal base resistivity bares further gain in efficiency potential. In order to understand the impact of the base resistivity and predict its optimal value, we performed additional ELBA analyses with varying base resistivity for the three HP mc-Si materials B-D. Both, the cell's direct dependence and the defect specific dependency on resistivity are considered. This is done by varying the resistivity in the solar cell model as well as in the experimentally obtained injection-dependent bulk lifetime data: A change in the base doping concentration does not change the defect concentrations, but still their recombination activity according to SRH statistics [20]. Assuming that the bulk lifetime is limited by deep SRH defects, the measured injection-dependent lifetime can be corrected for the varying base resistivity in first approximation by shifting it along the excess charge carrier density axis. Thus, we account for enhanced recombination at lower resistivities. We find an optimal resistivity in the range of 0.3–0.45 Ω cm for the three materials with respect to the TOPCon cell structure. The orange bars in Fig. 3(b) show the corresponding losses at the optimal resistivity, respectively. The enhanced recombination accounted for in the simulation is indicated by the bulk lifetime at MPP below each orange bar. Whereas material "B" still suffers from its poorer crystal quality, the losses of materials "C" and "D" can be reduced to ~ 0.4–0.5%$_{abs}$, which would result in efficiencies of ~ 22.6–22.7% for the investigated cell concept. We further see that the gain by an adapted resistivity is huge for material "C", whereas the efficiency potential of the material "D" is already nearly fully exploited, since its actual resistivity is close to the optimal resistivity. The slightly smaller losses for material "C" compared to material "D" after resistivity optimization suggest that our approach presented here does not sufficiently account for all effects that are associated with a change in resistivity: While enhanced recombination *via* deep SRH defects at lower resistivity is taken into account correctly, grain boundaries are treated in the same way in our predictions, as enhanced recombination at decorated grain boundaries is difficult to quantify exactly. This might lead to an uncertainty in the recombination activity of decorated grain boundaries at lower resistivity, which is also confirmed by the identification of loss mechanisms shown by the different parts of the orange bars in Fig. 3(b): The losses in the grains are identical for materials "C" and "D" after resistivity optimization, but we predict lower losses due to recombination-active structural crystal defects for material "C", which could be attributed to the uncertainty of increased recombination at grain boundaries for lower resistivity. The stronger injection-dependence of the inner-grain bulk lifetime of wafer "D" shown in Fig. 2(b) additionally suggests that the inner-grain lifetime in both materials is limited by different recombination mechanisms, as SRH recombination at identical defects would lead to the previously mentioned shift along the Δn axis only, which makes the suggested procedure less exact. However, this effect is negligible in terms of efficiency which is demonstrated by the identical losses in the grains in Fig. 3(b).

In order to understand the results for optimum resistivity in more detail, the efficiency is plotted as a function of base resistivity for material "C" in Fig. 4 (lower graph), showing the maximum at ~ 0.45 Ω cm. Additionally, the normalized cell parameters are plotted as a function of resistivity in the upper part of Fig. 4, demonstrating that the efficiency gains towards lower resistivities mainly stem from fill factor gains. Thus, shifting the resistivity of material "C" from the actual value of ~ 11 Ω cm to the optimal value of ~ 0.45 Ω cm would increase the fill factor by ~ 4% and the efficiency by 1%$_{abs}$. For very small resistivities, the efficiency drops again due to increasing Auger recombination, which leads to a strongly decreasing J_{sc}. It should be noted that the fill factor losses towards high resistivities are not a series resistance effect, but rather a recombination effect which influences V_{MPP} and also leads to losses in the pseudo fill factor. A perfect material only limited by intrinsic recombination would not be affected by this fill factor drop (red dashed curve in Fig. 4). However, the drop observed for material "C" is not an effect of an injection-dependent bulk lifetime: The two dotted curves show the simulated efficiency for a material with an injection-independent background lifetime of 3 ms (grey curve) and 1 ms (black curve), which demonstrates that the behavior observed for material "C" can already be explained by an injection-independent background limitation.

In contrast to the strong impact of the choice of base resistivity, we observe a weaker influence of wafer thickness on efficiency potential,

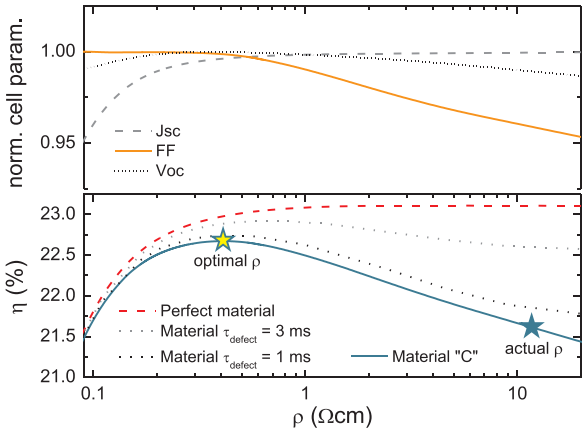

Fig. 4. Simulated influence of the base resistivity on the solar cell parameters for material "C". The increase towards lower resistivities until the maximum is due to an increase in the fill factor, while the decrease in the very low resistivity range is attributed to J_{sc}-limitations caused by Auger recombination. The decrease in efficiency towards high resistivity is not observed for perfect material without defect recombination, which is additionally included in the lower graph (red dashed curve). (For interpretation of the references to color in this figure legend, the reader is referred to the web version of this article).

Table 2
Cell parameters at STC for the record mc-Si solar cell ($2 \times 2\,cm^2$). Calibrated measurements by F-ISE CalLab.

V_{oc} (mV)	672.6
J_{sc} (mA/cm^2)	40.8
FF (%)	79.7
η (%)	**21.9**

which was analysed in a similar way by varying the thickness in the PC1D simulations in the ELBA analyses [21]. For the investigated material, maximum efficiencies can be achieved for a broad plateau of wafer thicknesses between 100 and 200 µm.

3.4. Solar cell results

Finally, we demonstrate the high efficiency potential of *n*-type HP mc-Si at the device level. Based on the material evaluations, we chose material "D" with the lowest base resistivity of 0.75 Ω cm for solar cell processing. We applied a TOPCon solar cell process sequence adapted for multicrystalline silicon [11]. The key features of this cell concept are the ultra-thin wet chemical SiO_x layer (~14 Å) grown at the rear side in combination with a 15 nm thick phosphorus-doped Si layer deposited on top of the SiO_x. This TOPCon layer stack provides a highly efficient passivating rear contact featuring an excellent interface passivation, an efficiently doped layer for maintaining the quasi-Fermi level separation, as well as an efficient majority carrier transport (for high fill factors) by tunneling through the ultra-thin oxide layer [22] and has been proven to be applicable to mc silicon substrate [10]. Additionally, a plasma-etched "black-silicon" front texture was applied in order to achieve low optical losses. The cell features a boron diffused emitter (90 Ω/sq) at the front side passivated by a stack of Al_2O_3 and SiN_x, evaporated Ti/Pd/Ag contacts at the front and a full area 1 µm thick Ag layer as rear side contact. Further details on the solar cell technology can be found in a separate publication [11]. The best solar cell features an efficiency of 21.9% confirmed by Fraunhofer ISE CalLab, which is the highest efficiency reported for a multicrystalline silicon solar cell. The cell parameters are listed in Table 2.

This result is in reasonable agreement with our efficiency prediction presented in section III.B for material "D". However, we still observe a difference of ~ 0.5%$_{abs}$ between the efficiency analysis by ELBA and the efficiency at the device level, mainly due a lower (pseudo) fill factor of the solar cell. We attribute this discrepancy to a yet unknown defect which is not accounted for in the simulation. A possible candidate is an interaction between structural crystal defects such as decorated grain boundaries and the emitter or the space charge region. An investigation of this effect together with a detailed loss analysis of the solar cell will be discussed in a future publication.

3.5. Further improvements

In future work, new HP mc-Si material with adapted resistivity and increased purity of the crucible system will be crystallized to reduce the material inherent limitations. In the solar cell process, we will include P-gettering to further increase the bulk lifetime as well as an optimized emitter for multicrystalline silicon. Together with an optional H-passivation of bulk defects, this will further enhance the efficiency of *n*-type mc-Si TOPCon solar cells. Thus, mc-Si solar cell efficiencies significantly exceeding 22% will be achievable in the near future.

4. Conclusion

In this contribution, we have shown how to reduce efficiency losses in *n*-type mc-Si solar cells by improvements of the material quality. Starting with material-related losses of more than 2%$_{abs}$ for standard *n*-type mc-Si, an improved crystal structure and diminished impact of impurities from the crystallization environment together with the optimal choice of parameters for base resistivity and thickness of the *n*-type mc-Si substrate reduce these losses to ~ 0.5%$_{abs}$. In combination with the high efficiency potential of the TOPCon cell concept, this enables efficiencies exceeding 22% on multicrystalline silicon substrates. These results were confirmed on actual devices with a new certified efficiency record for a multicrystalline silicon solar cell of 21.9%.

Acknowledgement

The authors would like to thank P. Häuber, F. Haas, F. Schätzle, A. Leimenstoll, S. Seitz, N. Brändlin, B. Steinhauser, K. Zimmermann, A. Seiler, E. Schäffer, and F. Martin for their support with processing and measurements. Also, the authors would like to thank Wacker Polysilicon for silicon materials and fruitful discussions.

This work was financially supported by the German Federal Ministry for Economic Affairs and Energy within the research project "multiTOP" under grant number 0324034.

References

[1] Y.M. Yang, A. Yu, B. Hsu, W.C. Hsu, A. Yang, C.W. Lan, Development of high-performance multicrystalline silicon for photovoltaic industry, Prog. Photo.: Res. Appl. 23 (3) (2013) 340–351.
[2] Trina Solar Press Release, Trina Solar Announces New Efficiency Record of 21.25% Efficiency for Multi-crystalline Silicon Solar Cell (accessed on 9 November 2015).
[3] M.A. Green, K. Emery, Y. Hishikawa, W. Warta, E.D. Dunlop, Solar cell efficiency tables (Version 47), Progress. Photovolt.: Res. Appl. 24 (1) (2016) 3–11.
[4] K. Yoshikawa, H. Kawasaki, W. Yoshida, T. Irie, K. Konishi, K. Nakano, T. Uto, D. Adachi, M. Kanematsu, H. Uzu, K. Yamamoto, Silicon heterojunction solar cell with interdigitated back contacts for a photoconversion efficiency over 26%, Nat. Energy 2 (2017) 17032.
[5] S.W. Glunz, F. Feldmann, A. Richter, M. Bivour, C. Reichel, H. Steinkemper, J. Benick, M. Hermle, The irresistible charm of a simple current flow pattern – 25% with a solar cell featuring a full-area back contact, in: Proceedings of the 31st EU PVSEC, Hamburg, Germany, 2015, pp. 259–263.
[6] D. Macdonald, L.J. Geerligs, Recombination activity of interstitial iron and other transition metal point defects in p- and n-type crystalline silicon, Appl. Phys. Lett. 85 (18) (2004) 4061–4063.
[7] J. Schmidt, K. Bothe, Structure and transformation of the metastable boron- and oxygen-related defect center in crystalline silicon, Phys. Rev. B 69 (2) (2004) 241071.
[8] J. Schmidt, A.G. Aberle, R. Hezel, Investigation of carrier lifetime instabilities in Cz-grown silicon, in: Proceedings of the 26th IEEE Photovoltaic Specialists Conference Anaheim, Anaheim, USA, 1997, pp. 13–18.
[9] F. Feldmann, M. Bivour, C. Reichel, M. Hermle, S.W. Glunz, Passivated rear contacts for high-efficiency n-type Si solar cells providing high interface passivation quality and excellent transport characteristics, Sol. Energy Mater. Sol. Cells 120 (2014) 270–274.
[10] F. Schindler, J. Schön, B. Michl, S. Riepe, P. Krenckel, J. Benick, F. Feldmann, M. Hermle, S.W. Glunz, W. Warta, M.C. Schubert, High-efficiency multicrystalline silicon solar cells: potential of n-Type doping, IEEE J. Photovolt. 5 (6) (2015) 1571–1579.
[11] J. Benick, A. Richter, R. Müller, H. Hauser, P. Krenckel, S. Riepe, F. Schindler, M.C. Schubert, M. Hermle, A. Bett, S.W. Glunz, High-Efficiency n-Type HP mc silicon solar cells, IEEE J. Photovolt. (2017) (Accepted).
[12] M.C. Schubert, J. Schon, F. Schindler, W. Kwapil, A. Abdollahinia, B. Michl, S. Riepe, C. Schmid, M. Schumann, S. Meyer, W. Warta, Impact of impurities from crucible and coating on mc-silicon quality—the example of iron and cobalt, IEEE J. Photovolt. 3 (4) (2013) 1250–1258.
[13] J.A. Giesecke, M.C. Schubert, B. Michl, F. Schindler, W. Warta, Minority carrier lifetime imaging of silicon wafers calibrated by quasi-steady-state photoluminescence, Sol. Energy Mater. Sol. Cells 95 (3) (2011) 1011–1018.
[14] D.A. Clugston, P.A. Basore, PC1D version 5: 32-bit solar cell modeling on personal computers, in: Proceedings of the 26th IEEE Photovoltaic Specialists Conference Anaheim, Anaheim, USA, 1997, pp. 207–210.
[15] H. Haug, J. Greulich, A. Kimmerle, E.S. Marstein, PC1Dmod 6.1 – state-of-the-art models in a well-known interface for improved simulation of Si solar cells, Sol. Energy Mater. Sol. Cells 142 (2015) 47–53.

[16] B. Michl, M. Rüdiger, J. Giesecke, M. Hermle, W. Warta, M.C. Schubert, Efficiency limiting bulk recombination in multicrystalline silicon solar cells, Sol. Energy Mater. Sol. Cells 98 (2012) 441–447.
[17] F. Schindler, B. Michl, J. Schön, W. Kwapil, W. Warta, M.C. Schubert, Solar cell efficiency losses due to impurities from the crucible in multicrystalline silicon, IEEE J. Photovolt. 4 (1) (2014) 122–129.
[18] W. Kwapil, J. Schön, W. Warta, M.C. Schubert, Carrier recombination at metallic precipitates in p- and n-type silicon, IEEE J. Photovolt. 5 (5) (2015) 1285–1292.
[19] H. Steinkemper, M. Hermle, S.W. Glunz, Comprehensive simulation study of industrially relevant silicon solar cell architectures for an optimal material parameter choice, Prog. Photo.: Res. Appl. 24 (10) (2016) 1319–1331.
[20] W. Shockley, W.T. Read Jr, Statistics of the recombinations of holes and electrons, Phys. Rev. 87 (5) (1952) 835–842.
[21] B. Michl, M. Kasemann, W. Warta, M.C. Schubert, Wafer thickness optimization for silicon solar cells of heterogeneous material quality, Phys. Status Solidi RRL 7 (11) (2013) 955–958.
[22] F. Feldmann, M. Bivour, C. Reichel, M. Hermle, S.W. Glunz, A passivated rear contact for high-efficiency n-type Si solar cells enabling high Voc's and FF > 82%, in: Proceedings of the 28th EU PVSEC, Paris, 2013, pp. 988–992.